

Effective population sizes for asymmetrically regulated birth-death processes

Yunbei Pan¹ and Tom Chou^{1,2}

¹*Department of Biomathematics, UCLA, Los Angeles, CA, 90095-1766, USA and*

²*Department of Mathematics, UCLA, Los Angeles, CA, 90095-1555, USA*

(Dated: July 2, 2026)

In multispecies birth-death processes, how population regulation—through suppressed replication, elevated mortality, or both—affects macroscopic stochastic dynamics has escaped detailed analysis. Here, we show that the distribution of regulation mechanisms can be invisible in deterministic or mean-field dynamics but play a significant role in the diffusive evolution of population frequencies. By introducing a tunable regulation partitioning parameter α_i and projecting a d -species birth-death process onto a $(d-1)$ -dimensional Moran process, we find a regulation-mechanism-dependent diffusion tensor. For the simple two-species case, we derive exact fixation times and probabilities to show how different regulation mechanisms stochastically favors a more birth-regulated species, even under complete deterministic neutrality. Our model also allows us to define an α -dependent effective population size $N_e(\alpha)$ among neutral species, generalizing its classical interpretation. For near-neutral populations or populations that are heterogeneous in their regulation mechanism, we used perturbation theory to calculate the spectral gap, identifying it with a diversity loss timescale which can also be interpreted as setting an effective population size. Our results are particularly applicable to interacting subpopulations of T cells (“clones”) which are near-neutral, are regulated through proliferation and apoptosis, and lose diversity with time.

Introduction - Stochastic models of the evolutionary dynamics of multiple interacting populations typically involve birth-death processes with nonlinear regulation effects and/or population constraints. The simplest and most foundational of such models are the Wright-Fisher model [1–4] and its continuous-time analogue, the Moran model [5]. A d -species birth-death process with strong total population regulation can be approximated by a $(d-1)$ -dimensional Moran model in which birth and death events are concerted to strictly fix the total population. Note that unlike Moran models on graphs [6–11], in which the order of the pair of birth and death events on connected nodes can lead to very different behavior such as fixation rates, we will consider a well-mixed population in which each birth and death are concerted.

Under a large-population “diffusion approximation,” the Wright-Fisher and Moran models can be expressed as a $(d-1)$ -dimensional Fokker-Planck equation with convection and diffusion coefficients that depend on the parameters of the underlying birth-death process [12–15]. In particular, the convection and diffusion coefficients describe the relative selection of certain species and geometric space explored by the population fractions. The diffusion term also allows one to define an effective population size that connects models that exhibit different variances in relative populations over time [16, 17]. For example, effective population sizes for more complex interactions and selection have been developed to relate discrete-time Wright-Fisher models to continuous-time Moran models.

Here, we demonstrate that a strong total population constraint (*e.g.*, a carrying capacity) not only allows a d -species birth-death process to be well approximated by a $(d-1)$ -dimensional Moran model, but that how the population regulation is implemented has an important effect on structure of the convection and diffusion terms in

its Fokker-Planck representation. A population may be regulated through reduced fecundity (birth regulation), elevated mortality (death-regulation), or some combination of both. These mechanisms are biologically distinct: resource limitation suppressing reproduction differs from density-dependent predation or crowding-induced mortality. A specific motivating example is the coexisting subpopulations of different T cells clones, each identified by different antigen receptors. While the total population is homeostatic [18, 19], under different conditions, signaling can increase replication and/or apoptosis [20–23]. For a birth-death process with linear density-dependent regulation, the equations governing expected populations are independent of whether regulation acts through birth, death, or any mixture thereof. The regulation mechanism reveals itself only in the stochastic dynamics (fluctuations) of the population(s) [24].

Following Constable and McKane [25, 26], we analyze $(d-1)$ -dimensional Moran model approximations to the d -dimensional birth-death process in the large population limit. The diffusion approximation leads to convection (“selection”) and diffusion (“drift”) terms that depend not only on the individual birth rates, death rates, and carrying capacity interaction matrix, but also on how carrying capacity is partitioned between birth and death for each species. Our results reveal how selection and the “drift” terms, through effective population sizes, depend on how carrying capacity regulation is implemented. By using a spectral decomposition, we extend the concept of effective population size to non-neutral systems in which species have different birth rates, death rates, and regulation terms. Our more general interpretation of effective population sizes applies to processes with separate birth and death events, nonlinear population regulation, and even weak non-neutrality, beyond its initial purpose

of matching a discrete-generation Wright-Fisher model with the continuous time Moran model.

Regulated birth-death model - We consider d -species with populations n_i , $i = 1, \dots, d$, collected in the state vector $\mathbf{n} = (n_1, \dots, n_d)$. The system evolves as a continuous-time Markovian birth-death process in which each species i undergoes independent birth and death events at population-regulated per-capita rates according to a Verhulst type model

$$\begin{aligned}\beta_i(\mathbf{n}) &= b_i \left(1 - \frac{\alpha_i}{K} \sum_{j=1}^d \gamma_{ij} n_j\right)^+ n_i, \\ \delta_i(\mathbf{n}) &= d_i \left(1 + \frac{(1-\alpha_i) b_i}{K d_i} \sum_{j=1}^d \gamma_{ij} n_j\right) n_i.\end{aligned}\quad (1)$$

Here, $(\cdot)^+ \equiv \max(\cdot, 0)$ enforces the non-negativity of the birth rate and $b_i > 0$ and $d_i > 0$ are the intrinsic (density-independent) per-capita birth and death rates of species i . The matrix $\gamma_{ij} \sim O(1)$ represents interspecies competition, while $K \gg 1$ sets the overall population size. Thus, K/γ_{ij} encodes the effective carrying capacity that species j imposes on species i . The parameter $\alpha_i \in [0, 1]$ controls how density-dependent regulation is partitioned between birth and death for species i : $\alpha_i = 1$ corresponds to pure birth-regulation (density suppresses fecundity while the death rate $\delta_i = d_i n_i$ remains density-independent), whereas $\alpha_i = 0$ corresponds to pure death-regulation (density elevates mortality while the birth rate is unregulated). The probability density over the population \mathbf{n} obeys the continuous-time master equation given in Eq. S1 of Appendix A in the Supplementary Material.

The key observation is that, when $\beta_i(\mathbf{n}) > 0$, the net rate,

$$\beta_i(\mathbf{n}) - \delta_i(\mathbf{n}) = (b_i - d_i) n_i - \frac{b_i}{K} \sum_{j=1}^d \gamma_{ij} n_j n_i, \quad (2)$$

is independent of α_i . Thus, the deterministic (mean-field) dynamics, obtained by replacing \mathbf{n} with its expectation, are completely blind to how regulation is distributed. In contrast, the total event rate,

$$\beta_i(\mathbf{n}) + \delta_i(\mathbf{n}) = (b_i + d_i) n_i + (1 - 2\alpha_i) \frac{b_i}{K} \sum_{j=1}^d \gamma_{ij} n_j n_i, \quad (3)$$

depends explicitly on α_i . Clearly, α_i affects the amplitude of demographic noise through the total event rate. With the same deterministic dynamics, density regulation through death rather than birth increases the turnover rate and produces stronger demographic fluctuations. An explicit demonstration of how the regulation parameter α_i arises only in higher moments of the population is shown in Appendix A.

Diffusion approximation and projection to frequency simplex - We henceforth restrict ourselves to parameter regimes in which $b_i > d_i$, such that typical populations approach a large carrying capacity, allowing us to apply a continuum or ‘‘diffusion’’ approximation (Eqs. S4 and S5 in Appendix B of the Supplementary Material.)

To isolate the effects of mean-field fitness from the microscopic noise geometry, we further assume all intrinsic birth and death rates $b_i, d_i \sim O(1)$ and the carrying capacity $K \gg 1$. Then, we consider three scenarios of parameter regimes: (i) a *fully neutral* limit in which $b_i = b$, $d_i = d$, $\gamma_{ij} = 1$, and $\alpha_i = \alpha$, (ii) a *semi-neutral* limit in which $b_i = b$, $d_i = d$, $\gamma_{ij} = 1$, with $\alpha_i \neq \alpha_j$ (for $j \neq i$), and (iii) a *quasi-neutral* case, where fitness and regulation differences are weak: $|b_i - b_j|, |d_i - d_j|, |\alpha_i - \alpha_j|, |\gamma_{ij} - 1| \leq O(1/K)$.

The full d -dimensional birth-death process admits a natural decomposition into a fast ‘‘ecological’’ variable u (rescaled total population) and slow ‘‘evolutionary’’ variables p_i (species frequencies)

$$u \equiv \frac{1}{K} \sum_{i=1}^d n_i, \quad p_i \equiv \frac{n_i}{\sum_{k=1}^d n_k}, \quad i = 1, \dots, d-1, \quad (4)$$

with $p_d = 1 - \sum_{i=1}^{d-1} p_i$. Consequently, the rescaled total population u is bounded above by $u_{\max}(\mathbf{p}) = \min_i \{1/(\alpha_i \sum_j \gamma_{ij} p_j)\}$. The frequencies $\mathbf{p} = (p_1, \dots, p_{d-1})$ live in the $(d-1)$ -simplex Δ^{d-1} . The domain $\mathcal{D} = \{(u, \mathbf{p}) \in \mathbb{R}_+ \times \Delta^{d-1} : 0 < u < u_{\max}(\mathbf{p})\}$ is thus bounded by a reflecting hypersurface $\partial\mathcal{D}_{\text{refl}} = \{(u, \mathbf{p}) : u = u_{\max}(\mathbf{p})\}$. A pure death-regulation model ($\alpha_i \rightarrow 0$) lives in an unbounded domain. The Fokker-Planck equation for the probability density $P(\mathbf{x}, t)$ (Eq. S4) is then transformed into one for the joint density $P(u, \mathbf{p}, t)$ given by Eqs. S6 and S7 in Appendix B.

Although the extinction point $u = 0$ is the true infinite-time equilibrium, on the $O(1)$ timescale, the rescaled total population u (the ecological variable) relaxes to a local, frequency-dependent quasi-equilibrium, $u^*(\mathbf{p}) = v(\mathbf{p})/R(\mathbf{p})$, where $v(\mathbf{p}) \equiv \sum_{i=1}^d (b_i - d_i) p_i = \bar{b}(\mathbf{p}) - \bar{d}(\mathbf{p})$ is the mean net growth rate and $R(\mathbf{p}) \equiv \sum_{i,j=1}^d b_i \gamma_{ij} p_i p_j$ is the competition-weighted birth rate. In contrast, the frequencies \mathbf{p} evolve on the slow timescale $O(1/K)$. By freezing \mathbf{p} , the local conditional dynamics of u is governed by convection $A_u = \sum_{i=1}^d (\beta_i - \delta_i)/K$ and diffusion $B_{uu}(u, \mathbf{p}) = \sum_{i=1}^d (\beta_i + \delta_i)/K$. In the vicinity of u^* , the linear restoring approximation $A_u \approx \partial_u A_u^* \cdot (u - u^*)$ balances the $O(1/K)$ demographic diffusion of magnitude $B_{uu}/(2K)$. The local dynamics of u thus reduce to an Ornstein-Uhlenbeck process with fluctuations of $O(1/\sqrt{K})$. In the decomposition $P(u, \mathbf{p}, t) = \rho(\mathbf{p}, t) \pi(u|\mathbf{p})$, the conditional quasi-stationary distribu-

tion (QSD) of u converges to a sharply peaked Gaussian

$$\pi(u|\mathbf{p}) \approx \mathcal{N}\left(u^*(\mathbf{p}), -\frac{B_{uu}^*(\mathbf{p})}{2K\partial_u A_u^*(\mathbf{p})}\right). \quad (5)$$

Integrating out u via the QSD yields the projected $(d-1)$ -dimensional Fokker–Planck equation for the marginal frequency density $\rho(\mathbf{p}, t)$,

$$\partial_t \rho(\mathbf{p}, t) + \sum_{i=1}^{d-1} \partial_{p_i} (A_i \rho) = \frac{1}{2K} \sum_{i,j=1}^{d-1} \partial_{p_i} \partial_{p_j} (B_{i,j} \rho), \quad (6)$$

which is a generalized “diffusion approximation” to a $(d-1)$ -dimensional Moran process with regulation-dependent coefficients. To leading order, $A_i \equiv A_i(u^*, \mathbf{p})$ and $B_{i,j} \equiv B_{i,j}(u^*, \mathbf{p})$ is evaluated at the quasi-equilibrium population u^* which is equivalent to recovering the hard total population constraint of the standard Moran model. Eq. 6 defines the operator $\mathcal{L}_\alpha^\dagger = -K \sum_{i=1}^{d-1} \partial_{p_i} (A_i \cdot) + (1/2) \sum_{i,j=1}^{d-1} \partial_i \partial_j (B_{i,j} \cdot)$ and its adjoint $\mathcal{L}_\alpha = K \sum_{i=1}^{d-1} A_i \partial_{p_i} + (1/2) \sum_{i,j=1}^{d-1} B_{i,j} \partial_i \partial_j$.

Regulation-induced convection. To more explicitly resolve the convection term, first define the population averaged intrinsic birth and death rates $\bar{b}(\mathbf{p}) \equiv \sum_{i=1}^d b_i p_i$ and $\bar{d}(\mathbf{p}) \equiv \sum_{i=1}^d d_i p_i$, the frequency-weighted mean regulation $\bar{\alpha}(\mathbf{p}) \equiv \sum_{i=1}^d \alpha_i p_i$, and the weighted interaction coefficient $\bar{\gamma}_i(\mathbf{p}) \equiv \sum_{j=1}^d \gamma_{ij} p_j$. In the $K \gg 1$ limit, the convection coefficient can be written as

$$\begin{aligned} A_i(\mathbf{p}) = & [(b_i - \bar{b}(\mathbf{p})) - (d_i - \bar{d}(\mathbf{p}))] p_i \\ & - u^*(\mathbf{p}) (b_i \bar{\gamma}_i(\mathbf{p}) - \sum_k b_k \bar{\gamma}_k(\mathbf{p}) p_k) p_i \\ & + \frac{2b}{K} (\alpha_i - \bar{\alpha}(\mathbf{p})) p_i + O(1/K^2). \end{aligned} \quad (7)$$

In addition to convection arising from differences in birth and death rates, there is a regulation-induced bias of order $O(1/K)$ due to heterogeneity in α_i . The convection $A_i(\mathbf{p})$ strictly vanishes under full neutrality.

Regulation-mediated diffusivity. The corresponding diffusion tensor can be written in the form

$$B_{i,j}(\mathbf{p}) = \sum_{k=1}^d (\mathbb{1}_{ik} - p_i)(\mathbb{1}_{jk} - p_j) p_k W_k(\mathbf{p}), \quad (8)$$

where $\mathbb{1}_{ik}$ is the Kronecker delta and the species-specific noise amplitude is denoted by

$$W_k(\mathbf{p}) \equiv \frac{b_k + d_k}{u^*(\mathbf{p})} + (1 - 2\alpha_k) b_k \bar{\gamma}_k(\mathbf{p}). \quad (9)$$

Rather than a uniform scalar variance, $W_k(\mathbf{p})$ explicitly summarizes the macroscopic demographic fluctuations arising from the parameters b_k , d_k , $\bar{\gamma}_k(\mathbf{p})$, and α_k .

Results - The evolutionary fate of the populations governed by Eqs. 8-9 is shaped by the structure of regulation-dependent demographic noise. The convection and diffusion terms in Eqs. 7, 8, and 9 can be further expanded in

powers of $1/K$ according to the limits of interest, *e.g.*, (i), (ii), or (iii). We will outline explicit results in a few select cases. For the fully regulated neutral case (i), the diffusion (genetic drift) is symmetric which allows the macroscopic fluctuations to be fully captured by a modified, α -dependent scalar effective population size $N_e(\alpha)$. In the semi-neutral limit (ii) with heterogeneous regulation α_i , we find explicit results for $d = 2$ (one-dimensional Moran model). In this case, symmetry-breaking regulation difference $\alpha_1 \neq \alpha_2$ gives rise to both convection and diffusion terms that are both $O(1/K)$ (an $O(1)$ “Peclet number”) but explicit α_1, α_2 -dependent expressions for mean fixation times and fixation probabilities are found. For more general, near-neutral cases (iii) and higher $d \geq 3$, analytic solutions are not available as species-specific regulation distorts the multidimensional geometry of genetic drift, precluding identification of a \mathbf{p} -independent scalar effective population size. In such cases, we propose characterizing the diversity loss as an overall measure of the renormalization of the diffusion tensor. We define an eigenvalue based interpretation of effective population size through the spectral gap, which can be computed numerically or through perturbation theory.

Fully neutral model and scalar $N_e(\alpha)$. In the fully neutral regime (i), the noise weight Eq. 9 becomes species-independent: $W_k \equiv W = (b + d)/u^* + (1 - 2\alpha)b$ where $u^* = (1 - d/b)$. The diffusion tensor Eq. 8 therefore reduces to an isotropic form $B_{i,j} = W p_i (\mathbb{1}_{ij} - p_j)$. Matching the diffusion coefficient $B_{i,j}/(2K)$ with that of the standard Wright–Fisher form $(b + d)p_i (\mathbb{1}_{ij} - p_j)/(2N_e)$ defines a dimensionless scalar effective population size:

$$N_e(\alpha) = \frac{\left(\frac{K}{2}\right)\left(1 - \frac{d^2}{b^2}\right)}{1 - \alpha\left(1 - \frac{d}{b}\right)} = \begin{cases} \frac{K}{2}\left(1 - \frac{d^2}{b^2}\right), & \alpha = 0 \\ \frac{K}{2}\left(\frac{b}{d}\right)\left(1 - \frac{d^2}{b^2}\right), & \alpha = 1. \end{cases} \quad (10)$$

Since $b > d > 0$ and $\alpha \in [0, 1]$, N_e strictly increases with α , with a value that can vary by up to a factor of b/d . The limits reveal a fundamental asymmetry: birth-regulated populations ($\alpha \rightarrow 1$) suppress replication through density feedback without introducing additional demographic events. This suppression results in an intrinsically lower total event rate and weaker genetic drift compared to regulation that increases the effective death rate. The total dynamic rate is chosen to be $b + d$ so that $N_e = K((1 - d/b))$ at $\alpha = 1/2$, when the regulation affects birth and death rates equally.

Nonuniform regulation: effective selection and fixation for $d = 2$. For $d = 2$, we can consider the more general near-neutral birth-death process and its associated one-dimensional Moran model defined by convection $A_1(p_1) = s_1(p_1)p_1(1 - p_1)$ and diffusion $B(p_1)$ expanded to $O(1/K)$ and $O(1)$, respectively:

$$\begin{aligned}
s_1(\mathbf{p}) &= (b_1 - b_2) - (d_1 - d_2) \\
&\quad - u^*(\mathbf{p}) [b_1 \bar{\gamma}_1(\mathbf{p}) - b_2 \bar{\gamma}_2(\mathbf{p})] \\
&\quad + \frac{2b}{K} (\alpha_1 - \alpha_2) + O(1/K^2)
\end{aligned} \tag{11}$$

and $B(p_1) = [(1 - p_1)W_1(p_1) + p_1W_2(p_1)]p_1(1 - p_1)$, where p_1 is the population fraction of species 1. In this one-dimensional model, one can derive analytic expressions for quantities such as the fixation probability and the mean time to fixation. To obtain simpler expressions that focus on how heterogeneity in regulation affects population dynamics, we restrict ourselves to the semi-neutral case (ii) in which $b_i = b, d_i = d, \gamma_{ij} = 1$ but α_1, α_2 are arbitrary. Then, the selection coefficient becomes $s_1 = \frac{2b}{K}(\alpha_1 - \alpha_2)$, and the diffusion to lowest order simplifies to a quadratic polynomial $B(p_1) = 2b [b/(b - d) - \alpha_1(1 - p_1) - \alpha_2 p_1] p_1(1 - p_1)$.

By integrating the exact backward equation, we obtain the closed-form fixation probability starting from an initial frequency $p_1(0) = p_0$:

$$q(p_0) = \frac{p_0(1 - \alpha_2 u^*)}{1 - u^* [(1 - p_0)\alpha_1 + p_0\alpha_2]}, \quad u^* = (1 - d/b), \tag{12}$$

satisfying the absorbing boundary conditions $q(0) = 0$ and $q(1) = 1$. This exact solution to the diffusion approximation recovers the macroscopic neutral expectation $q(p_0) = p_0$ when $\alpha_1 = \alpha_2$.

Fig. 1(a) shows that the species dominated by death regulation ($\alpha_i < 1/2$) experiences stronger fluctuations and is more likely to suffer extinction (lower fixation probability $q(p_0) < p_0$). Despite having no favorable selection, a birth regulation-dominated population ($\alpha_i > 1/2$) has a weaker demographic noise amplitude, giving rise to a fixation bias $q(p_0) > p_0$ for all $p_0 \in (0, 1)$, independent of K . Due to the numerator $p_0(1 - p_0)$, the fixation bias ($\sim O(1)$) exactly vanishes at the absorbing boundaries and peaks at an interior frequency, confirming that regulation-induced selection is a global geometric property instead of a local artifact. Fig. 1(b) shows a heatmap of the maximum fixation bias $q(1/2) - 1/2$ across regulation pairs (α_1, α_2) . The expected fixation times of species 1 conditioned on fixation $\mathbb{E}[T_1|p_0]$ can also be evaluated exactly using the conditioned backward operator, and is given in Appendix C. The result confirms that the stochastically favored birth-regulated species not only has a higher probability of fixation but also exhibits a faster fixation trajectory.

Nonuniform regulation in $d \geq 3$: Metric deformation in a conjugate representation. As we have seen, in non-neutral cases where a frequency-independent scalar N_e cannot be uniquely defined, fixation times and probabilities can in principle be computed. Another quantity related to population size in high-dimensional non-neutral cases is the ‘‘diversity loss rate’’ relative to the intrinsic diffusion rates $b_i + d_i$. This decay rate is defined through

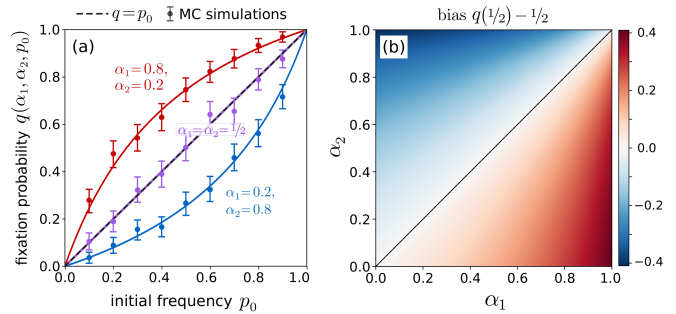


FIG. 1. Demographic noise asymmetry in $d = 2$ model modulates extinction fates. (a) The exact fixation probability $q(p_0)$ of species 1 as a function of its initial frequency p_0 . Despite zero mean-field fitness differences, regulation asymmetry ($\alpha_1 \neq \alpha_2$) shifts the fixation curves away from the classical neutral baseline $q(p_0) = p_0$ (dashed line). Closed-form analytical predictions (solid lines, Eq. 12) match results from discrete Gillespie simulations, validating the diffusion approximation and the resulting macroscopic fixation bias. (b) Heatmap of the maximum fixation bias $q(1/2) - 1/2$ for species 1 across regulation pairings (α_1, α_2) . The species with the larger α , relies relatively more on suppressed birth than elevated mortality, maintains a lower turnover rate, and is stochastically favored.

the spectral gap of the Fokker-Planck operator.

When $d \geq 3$ and regulation α is heterogeneous, the species-specific noise weights W_k distort the multidimensional geometry of diffusion. To evaluate the Fokker-Planck operator, either numerically or analytically, we first need to address the degeneracy of the diffusion tensor $B_{i,j}$ at the simplex boundaries $\{p_i = 0\}$, which destabilizes spatial discretization. Using $z_i \equiv \log(p_i/p_d)$, $-\infty \leq z_i \leq +\infty$, we map these boundaries to infinity; the diffusion tensor takes on the form

$$\tilde{B}_{i,j} = \frac{W_i}{p_i} \mathbb{1}_{ij} + \frac{W_d}{p_d} \tag{13}$$

and is strictly positive definite across the entire space. The frequencies $p_j(\mathbf{z})$ are implicitly soft-max functions of \mathbf{z} given in Appendix D. The \mathbf{p} and \mathbf{z} representations of the diffusion are conjugate and preserve the common spectral structure.

By decomposing $W_k(\mathbf{p}) \equiv \bar{W}(\mathbf{p}) + \Delta W_k(\mathbf{p})$, where $\bar{W} \equiv \sum_k p_k W_k$, the deformed metric directly inherits the rank-one perturbation structure:

$$\tilde{B}_{i,j} = \tilde{B}_{i,j}^{(0)} + \left(\frac{\Delta W_i}{p_i} \mathbb{1}_{ij} + \frac{\Delta W_d}{p_d} \right), \tag{14}$$

where $\tilde{B}_{i,j}^{(0)} = \bar{W} (\mathbb{1}_{ij}/p_i + 1/p_d)$ is the classical isotropic Fisher information metric recovered in the fully neutral limit ($W_k(\mathbf{p}) \equiv W$). This structured decomposition makes the regulation-induced asymmetry numerically tractable by permitting easy application of robust spatial discretization or adaptive spectral methods [27, 28], enabling direct computation of the smallest posi-

tive decay rate λ_1 for general values of α_i , which is equivalent to the negative of the leading nonzero eigenvalue of \mathcal{L}_α .

Degenerate perturbation and a spectral gap extension of effective population size. For weakly non-neutral cases, we can more conveniently perform perturbation analysis on the eigenvalues of the original Fokker-Planck operator \mathcal{L}_α using the form of $B_{i,j}(\mathbf{p})$ given in Eq. 8.

In the fully neutral case ($W_k \equiv W$ and $\Delta W_k \equiv 0$), the “unperturbed” backward operator $\mathcal{L}_\alpha^{(0)}$ acts on pairs of “modes”: $\mathcal{L}_\alpha^{(0)}(p_i p_j) = -W p_i p_j$ for any $i \neq j$. Hence, the smallest positive decay rate $\lambda_1^{(0)} = W$ is degenerate, spanned by the $d(d-1)/2$ -dimensional subspace of pairwise modes. While the exact decomposition $W_k = \bar{W} + \Delta W_k$ always holds, to provide tractable analytic expressions, we now restrict ourselves to the semi-neutral case with an additional constraint of weak regulation heterogeneity $|\alpha_i - \alpha_j| < O(1/K)$. The excess term can then be treated as a perturbation $\Delta W_k = \varepsilon W_k$ with $\varepsilon \sim 1/K$ arising from the differences $\alpha_i - \alpha_j$. This scaling ensures that the geometric perturbation to the demographic drift remains separated from deterministic finite-size effects.

Appendix D provides details on the perturbation analysis and shows the precise first-order splitting of the largest eigenvalue is

$$\lambda_{ij}^{(1)} = W_i + W_j - \left(\frac{1}{2}W_i + \frac{1}{2}W_j \right) = \frac{1}{2}(W_i + W_j), \quad (15)$$

where in this semi-neutral, weak heterogeneity case, $(1/2)W_i = b^2/(b-d) - b\alpha_i$, independent of \mathbf{p} .

The macroscopic diversity decay rate associated with $\lambda_{ij} = \lambda_1^{(0)} + \lambda_{ij}^{(1)}$ splits into $d(d-1)/2$ distinct levels. The global timescale of diversity loss T_{div} is determined by the slowest decaying mode, corresponding to the minimal spectral gap:

$$T_{\text{div}}^{-1} := \lambda_1 = \min_{i \neq j} \lambda_{ij} = \frac{1}{2} (W_i^{\min} + W_j^{\min}), \quad (16)$$

where W_i^{\min} and W_j^{\min} are the two smallest noise weights in the system. The exact closed-form expression for the diversity loss timescale can then be used to define an extinction-time-based spectral effective population size:

$$\begin{aligned} N_e^{\text{spec}}(\{\alpha_i\}) &= \frac{2(b+d)K}{W_i^{\min} + W_j^{\min}} \\ &= \frac{\left(\frac{K}{2}\right)\left(1 - \frac{d^2}{b^2}\right)}{1 - (1/2)(\alpha_i^{\max} + \alpha_j^{\max})\left(1 - \frac{d}{b}\right)}, \end{aligned} \quad (17)$$

where α_i^{\max} and α_j^{\max} are the two largest regulation parameters across all species. Eq. 17 generalizes the fully neutral effective population size $N_e(\alpha)$ to take into account weakly heterogeneous α_i and provides an $O(1)$ correction to Eq. 10. Additional validation and connection to macroscopic observables are detailed in **Appendix D** of the Supplementary Material.

Discussion and Conclusions - In this Letter, we demonstrated that the microscopic mechanisms regulating multispecies population densities are not merely ecological details that vanish upon averaging. They affect higher correlations and shape the geometry of the stochastic dynamics. Classical deterministic models often treat carrying capacity as a uniform constraint, resulting in mean-field dynamics that cannot resolve whether a population is regulated through suppressed fecundity or elevated mortality. By projecting the regulated birth-death dynamics into a frequency simplex of a diffusion approximation, we showed that heterogeneity in regulation mechanism introduces a frequency-dependent anisotropy in the demographic noise.

To lowest order, how regulation is implemented and its heterogeneity across species manifests itself in the diffusion tensor of the population fractions. The classical reduction of stochastic fluctuations to a single scalar holds strictly only under a fully neutral model, including perfectly homogeneous regulation mechanisms. The regulation-dependent diffusion amplitude defines a generalized effective population size $N_e(\alpha)$ which we derived in Eqs. 10. Once species-specific regulation mechanisms are introduced, the isotropy of the diffusion is broken. In diverse ecosystems ($d \geq 3$), the multidimensional structure of the noise splits the macroscopic relaxation timescales. The loss of diversity is therefore governed by a spectrum of decay rates that are determined by the heterogeneous regulation mechanism.

From a biological perspective, these findings show that birth-regulated populations possess an inherent stochastic advantage over death-regulated ones. By suppressing replication rather than elevating mortality under crowding, birth-regulated species maintain lower total event rates at the same carrying capacity, thereby experiencing weaker diffusion/genetic drift. This purely noise-induced mechanism provides a theoretical basis for understanding why certain resilient lineages, such as memory T cells or dormant microbial variants, might rely preferentially on division suppression rather than apoptosis to maintain homeostasis.

The spectral framework established here provides a mathematical foundation for the future exploration of non-neutral stochastic processes in higher dimensions. A promising direction of investigation is understanding how additional stochastic processes such as mutation and environmental noise (in *e.g.*, b_i, d_i, K) operate under heterogeneous regulation conditions influence diversity loss rates. Finally, our analysis assumed a linearly partitioned Verhulst mechanism (Eq. 1); how much of our findings persist with other forms of population regulation should be explored.

-
- [1] R. A. Fisher, Proceedings of the royal society of Edinburgh **42**, 321 (1923).
 - [2] T. D. Tran, J. Hofrichter, and J. Jost, Theory in Biosciences **132**, 73 (2013).
 - [3] R. A. Blythe and A. J. McKane, Journal of Statistical Mechanics: Theory and Experiment **2007**, P07018 (2007).
 - [4] W. J. Ewens and W. J. Ewens, *Mathematical population genetics: theoretical introduction*, Vol. 27 (Springer, 2004).
 - [5] P. A. P. Moran, in *Mathematical Proceedings of the Cambridge Philosophical Society*, Vol. 54 (Cambridge University Press, 1958) pp. 60–71.
 - [6] E. Lieberman, C. Hauert, and M. A. Nowak, Nature **433**, 312 (2005).
 - [7] J. Zukewich, V. Kurella, M. Doebeli, and C. Hauert, PLoS One **8**, e54639 (2013).
 - [8] K. Kaveh, N. L. Komarova, and M. Kohandel, Royal Society open science **2**, 140465 (2015).
 - [9] K. Kaveh, A. McAvoy, and M. A. Nowak, Royal Society open science **6**, 181661 (2019).
 - [10] J. Svoboda, S. Joshi, J. Tkadlec, and K. Chatterjee, PLoS Computational Biology **20**, e1012008 (2024).
 - [11] D. A. Brewster, Y. Huang, M. Mitzenmacher, and M. A. Nowak, arXiv preprint arXiv:2511.18252 (2025).
 - [12] M. Kimura, Journal of Applied Probability **1**, 177 (1964).
 - [13] A. Traulsen, J. C. Claussen, and C. Hauert, Physical Review Letters **95**, 238701 (2005).
 - [14] F. A. C. C. Chalub and M. O. Souza, Journal of Mathematical Biology **68**, 1089 (2014).
 - [15] A. J. Black and A. J. McKane, Trends in Ecology & Evolution **27**, 337 (2012).
 - [16] K. S. Korolev, M. Avlund, O. Hallatschek, and D. R. Nelson, Reviews of Modern Physics **82**, 1691 (2010).
 - [17] T. Chotibut and D. R. Nelson, Journal of Statistical Physics **167**, 777 (2017).
 - [18] C. D. Surh and J. Sprent, Immunity **29**, 848 (2008).
 - [19] B. Min, Frontiers in immunology **9**, 547 (2018).
 - [20] J. Hataye, J. J. Moon, A. Khoruts, C. Reilly, and M. K. Jenkins, Science **312**, 114 (2006).
 - [21] K. S. Schluns and L. Lefrançois, Nature Reviews Immunology **3**, 269 (2003).
 - [22] S. I. Mannering, J. Zhong, and C. Cheers, Immunology **106**, 87 (2002).
 - [23] A. Mayer, Y. Zhang, A. S. Perelson, and N. S. Wingreen, Proceedings of the National Academy of Sciences **116**, 5914 (2019).
 - [24] T. Chotibut and D. R. Nelson, Physical Review E **92**, 022718 (2015).
 - [25] G. W. A. Constable and A. J. McKane, Physical Review Letters **114**, 038101 (2015).
 - [26] G. W. A. Constable and A. J. McKane, Physical Review E **96**, 022416 (2017).
 - [27] M. Xia, S. Shao, and T. Chou, SIAM Journal on Scientific Computing **43**, A3244 (2021).
 - [28] T. Chou, S. Shao, and M. Xia, Applied Numerical Mathematics **183**, 201 (2023).

Supplementary Material

Appendix A: Master equation and mean-field ODEs

We consider a d -dimensional continuous-time Markovian birth-death process. Generally, regulation in a birth-death process manifests itself in population-dependent birth and death rates of each species i . Assuming a Markovian birth-death process of a system in state n_i , $i = 1, \dots, d$, the birth and death rates may be written as $\beta_i(\mathbf{n})$ and $\delta_i(\mathbf{n})$, and the probability $\mathbb{P}(\mathbf{n}, t)$ obeys the forward master equation

$$\frac{\partial \mathbb{P}(\mathbf{n}, t)}{\partial t} = \sum_i \left[\mathbb{A}_i^- (\beta_i \mathbb{P}) + \mathbb{A}_i^+ (\delta_i \mathbb{P}) - (\beta_i + \delta_i) \mathbb{P} \right], \quad (\text{S1})$$

where \mathbb{A}_i^\pm are the raising and lower operators on the i^{th} species population n_i . This master equation can be transformed into more tractable forms when *e.g.*, the birth and death rates lead to large populations allowing continuum approximations. Alternatively, exact ODEs describing the evolution of moments can be derived.

Using Eq. 1 and by applying the raising and lowering operators of the master equation, the exact evolution of the expected populations is governed by

$$\frac{d\mathbb{E}[n_i]}{dt} = (b_i - d_i)\mathbb{E}[n_i] - \frac{b_i}{K} \sum_j \mathbb{E}[n_i n_j]. \quad (\text{S2})$$

Neglecting correlations and approximating $\mathbb{E}[n_i n_j] \approx \mathbb{E}[n_i]\mathbb{E}[n_j]$ yields deterministic ODEs for $\mathbb{E}[n_i(t)]$. Crucially, the dependence on α_i strictly vanishes in the first moment, demonstrating that deterministic (mean-field) selection is entirely blind to the distribution of the regulation mechanism.

Dependences on the regulation mechanism α_i arise in the second moments which evolve according to

$$\begin{aligned} \frac{d\mathbb{E}[n_i n_j]}{dt} &= \mathbb{E}[n_j(\beta_i(\mathbf{n}) - \delta_i(\mathbf{n}))] + \mathbb{E}[n_i(\beta_j(\mathbf{n}) - \delta_j(\mathbf{n}))] + \mathbb{1}_{ij}\mathbb{E}[\beta_i(\mathbf{n}) + \delta_i(\mathbf{n})] \\ &= (b_i - d_i + b_j - d_j)\mathbb{E}[n_i n_j] - \frac{1}{K} \sum_\ell (b_i \gamma_{i\ell} + b_j \gamma_{j\ell})\mathbb{E}[n_i n_j n_\ell] \\ &\quad + \mathbb{1}_{ij} \left[(b_i + d_i)\mathbb{E}[n_i] + (1 - 2\alpha_i)\frac{b_i}{K} \sum_\ell \gamma_{i\ell}\mathbb{E}[n_i n_\ell] \right] \end{aligned} \quad (\text{S3})$$

where $\mathbb{1}_{ij}$ is the Kronecker delta function. Note that the last term depends on the regulation mechanism α_i . When is the choice of regulation important and how does it translate to $(d-1)$ -dimensional approximations (Moran models) in the large $K_{i\ell}$ limit? We answer these and related questions by investigating how stochasticity and differences in regulation mechanisms reveal themselves under different relevant limits.

Appendix B: Diffusion approximation and Moran limit of the birth-death process

To resolve the demographic fluctuations where α_i manifests, we take the large K limit and define the continuum state $\mathbf{x} = \mathbf{n}/K$. Truncating the Kramers-Moyal expansion at the second order yields the continuum Fokker-Planck equation:

$$\partial_t P(\mathbf{x}, t) + \sum_{i=1}^d \partial_{x_i} [\mu_i(\mathbf{x})P] = \frac{1}{2K} \sum_{i=1}^d \partial_{x_i}^2 [\sigma_i^2(\mathbf{x})P], \quad (\text{S4})$$

where the deterministic drift and demographic variance are

$$\begin{aligned}\mu_i(\mathbf{x}) &:= \frac{1}{K}(\beta_i(\mathbf{x}K) - \delta_i(\mathbf{x}K)) = (b_i - d_i)x_i - b_i \sum_{j=1}^d \gamma_{ij}x_i x_j \\ \sigma_i^2(\mathbf{x}) &:= \frac{1}{K}(\beta_i(\mathbf{x}K) + \delta_i(\mathbf{x}K)) = (b_i + d_i)x_i + b_i(1 - 2\alpha_i) \sum_{j=1}^d \gamma_{ij}x_i x_j.\end{aligned}\tag{S5}$$

To isolate the evolutionary dynamics, we transform the subpopulation \mathbf{x} into a total population variable $u = \sum_i x_i$ and the frequency variables $p_i = x_i/u$ for $i = 1, \dots, d-1$ (Eq. 4). By applying Itô's lemma, the fully coupled joint Fokker-Planck equation for $P(u, \mathbf{p}, t)$ becomes

$$\begin{aligned}\partial_t P(u, \mathbf{p}) + \partial_u (A_u P) + \sum_i \partial_{p_i} (A_i P) \\ = \frac{1}{2K} \left[\partial_u^2 (B_{uu} P) + 2 \sum_i \partial_{u, p_i}^2 (B_{u, i} P) + \sum_{i, j} \partial_{p_i, p_j}^2 (B_{i, j} P) \right],\end{aligned}\tag{S6}$$

where the transformed drift and diffusion coefficients are:

$$\begin{aligned}A_u(u, \mathbf{p}) &= \sum_{i=1}^d \mu_i(u\mathbf{p}), \quad B_{uu}(u, \mathbf{p}) = \sum_{i=1}^d \sigma_i^2(u\mathbf{p}) \\ A_i(u, \mathbf{p}) &= \sum_{k=1}^d (\mathbb{1}_{ik} - p_i) \left(\frac{\mu_k(u\mathbf{p})}{u} - \frac{\sigma_k^2(u\mathbf{p})}{Ku^2} \right) \\ B_{u, i}(u, \mathbf{p}) &= \frac{1}{u} \sum_{k=1}^d (\mathbb{1}_{ik} - p_i) \sigma_k^2(u\mathbf{p}) \\ B_{i, j}(u, \mathbf{p}) &= \frac{1}{u^2} \sum_{k=1}^d (\mathbb{1}_{ik} - p_i)(\mathbb{1}_{jk} - p_j) \sigma_k^2(u\mathbf{p}).\end{aligned}\tag{S7}$$

After eliminating the fast variable u , we find the regulation-mediated diffusion approximation to a $(d-1)$ -dimensional Moran model described by Eq. 6. Note that in the text, we defined the species-specific noise amplitude in Eq. 9 by $W_k(\mathbf{p}) \equiv \sigma_k^2(u^*\mathbf{p}) / (u^*(\mathbf{p}))^2$.

Appendix C: Two-species fixation and exact conditional mean first passage time

For $d = 2$, the backward equation $KA_1 q' + \frac{1}{2}Bq'' = 0$ yields the exact fixation probability $q(p_0) = \int_0^{p_0} \psi(x)dx / \int_0^1 \psi(x)dx$, $\psi(x) = \exp[-2K \int^x (A_1(y)/B(y))dy]$. On the semi-neutral case with heterogeneity in only α_i , the integrand $2KA_1/B$ is a ratio of quadratic polynomials. Its exact integration yields logarithmic functions that, upon exponentiation into $\psi(x)$, completely algebraically cancel, resulting in the exact rational function in Eq. (12).

To evaluate the expected time to fixation for species 1 conditioned on fixation, we apply the Doob h -transform to the backward Fokker-Planck operator \mathcal{L}_α . Conditioned on reaching the absorbing boundary at $p_0 = 1$, the process is governed by the transformed operator:

$$\mathcal{L}_\alpha^{\text{cond}} = \frac{1}{q(p_0)} \mathcal{L}(q(p_0) \cdot)\tag{S8}$$

Since the fixation probability satisfies the steady-state equation $\mathcal{L}q(p_0) = 0$, expanding the product rule reduces the conditioned operator to:

$$\mathcal{L}_\alpha^{\text{cond}} = \frac{1}{2}B(p_0)\partial_{p_0}^2 + \left(A(p_0) + B(p_0)\frac{\partial_{p_0}q(p_0)}{q(p_0)} \right) \partial_{p_0} \quad (\text{S9})$$

The conditional mean first passage time, $\mathbb{E}[T|p_0]$, satisfies the governing equation $\mathcal{L}^{\text{cond}}\mathbb{E}[T|p_0] = -1$, subject to the boundary conditions that it vanishes at the absorbing target ($\mathbb{E}[T|1] = 0$) and remains finite as $p_0 \downarrow 0$.

Given that $\mathcal{L}q(p_0) = 0$, we have

$$\frac{1}{2}B(p_0) \left[\partial_{p_0}^2 \mathbb{E}[T|p_0] + \left(2\frac{\partial_{p_0}q(p_0)}{q(p_0)} - \frac{\partial_{p_0}^2q(p_0)}{\partial_{p_0}q(p_0)} \right) \partial_{p_0} \mathbb{E}[T|p_0] \right] = -1. \quad (\text{S10})$$

Applying the absorbing boundary condition $\mathbb{E}[T|1] = 0$, we find

$$\mathbb{E}[T|p_0] = \int_{p_0}^1 \frac{\partial_y q(y)}{q^2(y)} \left(\int_0^y \frac{2q^2(x)}{B(x)\partial_x q(x)} dx \right) dy, \quad (\text{S11})$$

which using Fubini's theorem becomes

$$\mathbb{E}[T|p_0] = \int_0^{p_0} \frac{2q(x)}{B(x)\partial_x q(x)} \left(\frac{1-q(p_0)}{q(p_0)} \right) dx + \int_{p_0}^1 \frac{2(1-q(x))}{B(x)\partial_x q(x)} dx. \quad (\text{S12})$$

These integrals can be evaluated to

$$\begin{aligned} \mathbb{E}[T|p_0] = & \frac{1}{b\left(\frac{1}{u^*} - \alpha_2\right)} \left[\frac{\frac{1}{u^*} - \alpha_1}{\alpha_1 - \alpha_2} \ln \left(\frac{\frac{1}{u^*} - \alpha_2}{\frac{1}{u^*} - \alpha_1} \right) - \frac{\frac{1}{u^*} - \alpha_1}{p_0(\alpha_1 - \alpha_2)} \ln \left(\frac{\frac{1}{u^*} - \alpha_1(1-p_0) - \alpha_2 p_0}{\frac{1}{u^*} - \alpha_1} \right) \right. \\ & \left. + \ln \left(\frac{\frac{1}{u^*} - \alpha_2}{\frac{1}{u^*} - \alpha_1(1-p_0) - \alpha_2 p_0} \right) + \left(1 - \frac{1}{p_0} \right) \ln(1-p_0) \right]. \end{aligned} \quad (\text{S13})$$

Appendix D: Perturbation analysis of weakly deformed diffusion

To transform the Moran operator into a form more amenable to perturbation analysis, we map the simplex interior Δ_0^{d-1} diffeomorphically onto \mathbb{R}^{d-1} via the log-ratio coordinates: $z_i \equiv \log(p_i/p_d)$, $i = 1, \dots, d-1$. By Itô's calculus, the transformed diffusion tensor $\tilde{B}_{i,j} = \sum_{k,\ell} (\partial z_i / \partial p_k) (\partial z_j / \partial p_\ell) B_{k,\ell}$ analytically simplifies, collapsing into the strictly positive-definite, diagonal-plus-rank-one structure as given by Eq. 13

$$\tilde{B}_{i,j}(\mathbf{z}) = \frac{W_i(\mathbf{z})}{p_i(\mathbf{z})} \mathbb{1}_{ij} + \frac{W_d(\mathbf{z})}{p_d(\mathbf{z})}, \quad (\text{S14})$$

where $p_i(\mathbf{z})$ are explicitly

$$p_i(\mathbf{z}) = \frac{e^{z_i}}{1 + \sum_{j=1}^{d-1} e^{z_j}}, \quad p_d(\mathbf{z}) = \frac{1}{1 + \sum_{j=1}^{d-1} e^{z_j}} \quad (\text{S15})$$

In this representation, the corresponding backward Fokker-Planck operator, $\tilde{\mathcal{L}}_\alpha$, avoids finite-boundary singularities and can be resolved using spectral methods. The convection also accrues a geometric correction, $\tilde{A}_i = \sum_k (\partial z_i / \partial p_k) A_k + \frac{1}{2K} \sum_{k,\ell} (\partial^2 z_i / \partial p_k \partial p_\ell) B_{k,\ell}$.

Beside permitting easier numerical solutions (for low dimensions d) the \mathbf{p} and \mathbf{z} representations of the diffusion are conjugate and also preserve the common spectral structure. Thus, for the eigenvalues, we perform the perturbation analysis by evaluating the action on the original backward operator \mathcal{L}_α . In the fully neutral case ($W_k \equiv W$ and $\Delta W_k \equiv 0$), the unperturbed backward operator $\mathcal{L}_\alpha^{(0)}$ acts on the pairwise modes according to $\mathcal{L}_\alpha^{(0)}(p_i p_j) = -W p_i p_j$ for any $i \neq j$. Hence, the smallest positive decay rate $\lambda_1^{(0)} = W$ is degenerate, spanned by the $d(d-1)/2$ -dimensional subspace of pairwise modes.

By decomposing $W_k(\mathbf{p}) \equiv \bar{W}(\mathbf{p}) + \Delta W_k(\mathbf{p})$, where $\bar{W} \equiv \sum_k p_k W_k$, the deformed metric directly inherits the rank-one perturbation structure:

$$\tilde{B}_{i,j} = \tilde{B}_{i,j}^{(0)} + \left(\frac{\Delta W_i}{p_i} \mathbb{1}_{ij} + \frac{\Delta W_d}{p_d} \right), \quad (\text{S16})$$

where $\tilde{B}_{i,j}^{(0)} = W(\mathbb{1}_{ij}/p_i + 1/p_d)$ is the classical isotropic Fisher information metric recovered in the fully neutral limit ($W_k(\mathbf{p}) \equiv W$). This structured decomposition makes the regulation-induced asymmetry analytically tractable.

To be analytically explicit, we consider the weak regulation asymmetry regime $|\alpha_i - \alpha_j| \leq O(1/K)$. While the exact decomposition $W_k = \bar{W} + \Delta W_k$ always holds, we now restrict the magnitude of the heterogeneity such that $\Delta W_k = \varepsilon W_k$ with $\varepsilon \sim 1/K$ arising from the differences $\alpha_i - \alpha_j$. This scaling ensures that the geometric perturbation to the demographic drift remains separated from deterministic finite-size effects. Applying the perturbed operator $\mathcal{L}_\alpha = \mathcal{L}_\alpha^{(0)} + \varepsilon \mathcal{L}_\alpha^{(1)}$ to the pairwise modes yields

$$\mathcal{L}_\alpha(p_i p_j) = -p_i p_j \left[W + \varepsilon \left(W_i + W_j - \sum_{k=1}^d p_k W_k \right) \right]. \quad (\text{S17})$$

The presence of the cubic term ($p_i p_j p_k$) breaks the closure of the unperturbed quadratic subspace, coupling the pairwise modes to higher-order polynomials. Standard non-degenerate theory fails.

Thus, degenerate perturbation theory is introduced by projecting the perturbation operator $\mathcal{L}_\alpha^{(1)}$ onto the $d(d-1)/2$ -dimensional degenerate subspace to construct a secular matrix. We define the biorthogonal basis formed by the unperturbed right (backward) eigenfunctions $|\psi_{ab}^{(0)}\rangle = p_a p_b$ and the conjugate left (forward) eigenfunctions $\langle \phi_{ij}^{(0)}|$, satisfying $\langle \phi_{ij}^{(0)} | \psi_{ab}^{(0)} \rangle = \mathbb{1}_{(ij),(ab)}$. The eigenvalue problem $\det(\mathcal{L}_\alpha^{(1)} - \lambda_1^{(1)}) = 0$ constructs the secular matrix. The first-order corrections are the eigenvalues of the secular matrix with elements $\mathcal{L}_{\alpha, \{(ij),(ab)\}}^{(1)} = \langle \phi_{ij}^{(0)} | \mathcal{L}_\alpha^{(1)} | \psi_{ab}^{(0)} \rangle$.

Because the system possesses strictly absorbing boundaries without mutation, the left eigenfunction $\langle \phi_{ij}^{(0)}|$ projects any state onto the invariant $i-j$ boundary sub-manifold. Any polynomial containing a variable p_k where $k \notin \{i, j\}$ evaluates to zero under this projection. Consequently, for any $(a, b) \neq (i, j)$, the projection of the cubic term $\langle \phi_{ij}^{(0)} | p_a p_b p_k \rangle$ vanishes and the secular matrix is therefore diagonal.

To evaluate the diagonal elements $\mathcal{L}_{\alpha, \{(ij),(ij)\}}^{(1)}$, we utilize the algebraic closure on the $i-j$ boundary, where $p_i + p_j = 1$. The cubic projection simplifies as $\langle \phi_{ij}^{(0)} | p_i^2 p_j \rangle + \langle \phi_{ij}^{(0)} | p_i p_j^2 \rangle = \langle \phi_{ij}^{(0)} | p_i p_j (p_i + p_j) \rangle = \langle \phi_{ij}^{(0)} | p_i p_j \rangle = 1$. By the intrinsic exchange symmetry of the unperturbed operator, the individual projections must be equal, yielding $\langle \phi_{ij}^{(0)} | p_i^2 p_j \rangle = 1/2$.

To connect this spectral gap to macroscopic observables, we monitor the empirical pairwise heterozygosity $H(\tau) = \sum_{i < j} \langle p_i(\tau) p_j(\tau) \rangle$ over the rescaled time $\tau = t/K$. Because $H(\tau)$ is a linear combination of the pairwise modes, its long-time behavior is strictly governed by the minimal spectral gap, decaying asymptotically as $H(\tau) \sim \exp(-\lambda_1 \tau)$. For systems with strong heterogeneous

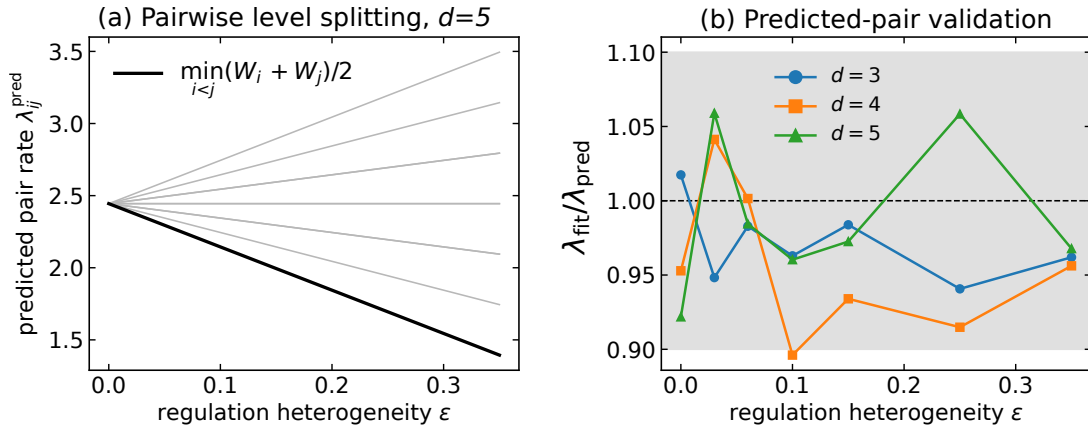


FIG. S1. **Spectral gap splitting and the macroscopic timescale of diversity loss.** (a) Analytical prediction of the first-order kinetic splitting for a $d = 5$ system. As regulation heterogeneity ε increases, the initially $d(d-1)/2$ -fold degenerate macroscopic decay rate smoothly splits into distinct pairwise levels. The global timescale of diversity loss is governed by the minimal spectral gap (thick black line), corresponding to the pair with the lowest aggregate turnover rate. (b) Validation of the degenerate perturbation theory under heterogeneous regulation ($\varepsilon > 0$). The ratio of the simulated spectral gap λ_{fit} to the analytically predicted gap $\lambda_{\text{pred}} = \frac{1}{2}(W_{\min} + W_{\min})$ remains near unity (mostly within the $\pm 10\%$ gray shaded region). This confirms that the macroscopic bottleneck of diversity loss is precisely captured by projecting the metric distortion onto the pairwise subspace.

regulation ($\varepsilon \sim O(1)$), the macroscopic timescale is completely sliced apart into distinct pairwise levels as shown in Fig. S1(a). The degenerate perturbation theory accurately captures this metric distortion: the ratio of the simulated decay rates to our analytical predictions tightly bounds around unity (Fig. S1(b)). The overall rate of diversity loss is governed by the mutually compatible species with the lowest total event rates (the pair minimizing $W_i + W_j$), preventing the ecosystem from rapid demographic collapse.